Online Hierarchical Volt/var Control for Unbalanced Distribution Networks Using Diagonal-scaling Alternating Direction Method of Multipliers

Heshi Wang, *Student Member*, *IEEE*, Wenxia Liu, *Member*, *IEEE*, Rui Cheng, *Member*, *IEEE*, Fuxin Wang, and Tianlong Wang, *Student Member*, *IEEE*

***Abstract*—This paper proposes an online hierarchical volt/var control (VVC) for unbalanced distribution networks using diagonal-scaling alternating direction method of multipliers (DS-ADMM). Under the hierarchical VVC strategy, local photovoltaic (PV) agents only exchange limited information with the center agent and adjust reactive power outputs in real time, with the goal of minimizing the voltage deviations and reactive power regulation costs in the time-varying environment. A diagonalized auxiliary matrix is constructed and developed from the Hessian matrix using preconditioning methods, which is then combined with alternating direction method of multipliers (ADMM) to design the DS-ADMM with improved convergence speed. The DS-ADMM is applied to the hierarchical VVC strategy, further improving the tracking capability and performance for time-varying environmental changes. Simulation studies on a modified IEEE 123-bus unbalanced distribution network are conducted to verify the effectiveness of the hierarchical VVC strategy using DS-ADMM and its robustness under non-ideal communication conditions, and its scalability is further validated on the modified IEEE 8500-node test feeder.**

***Index Terms*—Volt/var control (VVC), alternating direction method of multipliers (ADMM), photovoltaic (PV), reactive power, distribution network.**

I. Introduction

In recent years, the penetration of distributed energy resources (DERs) such as photovoltaic (PV) in distribution networks has been increasing, which has shifted the power flow in distribution networks from the traditional unidirectional pattern to a bidirectional pattern. Simultaneously, based on PV output data with minute-scale resolution, [1] and [2] reveal that PV generation exhibits significant rapid fluctuations. The uncertain and intermittent power outputs of DERs pose great challenges to the operation of distribution networks, exacerbating voltage quality and violation problems [3]. Traditional voltage control devices, e. g., on-load tap changers (OLTCs), are limited by response speed and switching frequency, making them ineffective to cope with rapid voltage fluctuations and violations in distribution networks [4], [5]. Meanwhile, with the rapid development of modern information, communication, and electronics technologies, there has been growing interest in utilizing smart inverters with fast frequency controls and reactive power support capabilities to design volt/var control (VVC) strategies for distribution networks [6]-[9].

Existing studies on the VVC strategies are generally categorized into two paradigms: data-driven strategies and model-based strategies. Data-driven VVC strategy typically avoids solving the VVC optimization problem and directly outputs the corresponding control decisions based on the required system states. A well-trained deep learning power flow (DLPF) model, as presented in [10], establishes an end-to-end mapping between system state parameters and power flow results. The DLPF model circumvents the computational complexity arising from the convex relaxation of power flow constraints in VVC optimization problem. Reference [11] employs a data-driven VVC strategy based on deep neural network (DNN) to rapidly estimate bus voltage sensitivities with respect to active/reactive power injections, thus enabling corresponding adjustments in inverter active/reactive power control rules. References [12]-[14] employ deep reinforcement learning techniques to solve the VVC optimization problem, aiming to determine the control actions of various voltage regulation devices. Specifically, an actor-critic algorithm with a Bayesian optimization framework is integrated in [12] to efficiently generate optimal VVC strategy. Reference [13] proposes a consensus-based multi-agent reinforcement learning framework to coordinate the actions of voltage regulators, OLTCs, and capacitors. In [14], the backward-forward sweep method is used to obtain accurate pow-

Manuscript received: January 23, 2025; revised: May 22, 2025; accepted: July 3, 2025. Date of CrossCheck: July 3, 2025. Date of online publication: September 18, 2025.

This work was supported by the Fundamental Research Funds for the Central Universities (No. 2024MS001), the Fellowship of the China Postdoctoral Science Foundation (No. 2024M750892), and the Postdoctoral Fellowship Program of CPSF (No. GZC20230785).

This article is distributed under the terms of the Creative Commons Attribution 4.0 International License (http://creativecommons.org/licenses/by/4.0/).

H. Wang, W. Liu, R. Cheng (corresponding author), F. Wang, and T. Wang are with the School of Electric and Electronic Engineering, North China Electric Power University, Beijing, China (e-mail: 15124491396@163.com; liuwenxia001@163.com; ruicheng@ncepu.edu.cn; wangfuxinariel@163.com; 120232101089@ncepu.edu.cn).

DOI: 10.35833/MPCE.2025.000070

er flow solutions for unbalanced three-phase systems, based on which an intelligent deep Q-network (DQN) framework is developed to solve the VVC optimization problem. However, data-driven VVC strategies generally operate as black-box models, offering limited insight into the underlying control mechanisms. The lack of interpretability and physical grounding reduces their credibilities and makes it challenging to guarantee consistent and reliable operation under diverse practical scenarios. Consequently, their applicabilities in real-world distribution networks are significantly constrained.

The model-based VVC strategies can be further categorized into three types according to the differences in communication architecture and decision-making entities: ① centralized VVC strategies; ② local VVC strategies; and ③ distributed VVC strategies. Centralized VVC strategies determine all controllable resources to achieve global optimal control performance for distribution networks [15]. However, centralized VVC strategies require the central processor to handle all computational tasks, demanding large amounts of private information and suffering from poor scalability [16], [17]. Local VVC strategies individually adjust controllable resources based on local measurement data without the need for any information exchange among nodes [18], [19]. Nevertheless, due to the lack of coordination mechanisms among controllable resources, local VVC strategies always fail to achieve the excellent optimal control performance [20], [21].

As a compromise between centralized and local VVC strategies, distributed VVC strategies exhibit great scalability, superb control performance, and privacy-respecting properties [22]. Studies in [23]-[26] design fully distributed VVC strategies based on the classical alternating direction method of multipliers (ADMM) (corresponding to distributed VVC strategies using ADMM), with the objective of minimizing either voltage deviations or network losses. The distributed VVC strategies in [23] - [26] rely on the information exchange among neighboring nodes. Additionally, hierarchical distributed VVC strategies are proposed in [27] and [28], which rely on the communication and collaboration between the center and local agents. However, the aforementioned distributed VVC strategies and hierarchical distributed VVC strategies using ADMM are mostly implemented in an offline manner, meaning their VVC decisions cannot be applied to the distribution networks till the iteration convergences. This limitation may render them ineffective in capturing rapid fluctuations in distribution networks caused by the high variability of DERs.

Instead, online VVC strategies have received increasing attention in recent years. The online VVC strategies adjust the decision/control variables in real time based on the real-time measurements to adapt to the dynamic conditions without the need for convergence [29], [30]. ADMM and dual ascent methods are enhanced and applied to develop online VVC strategies by controlling the reactive power outputs of inverters [31], [32]. Reference [31] addresses the issue of inaccurate DER generation forecasting by designing an online microgrid energy management strategy based on ADMM. In [32], an online voltage control strategy is proposed by including the voltage feedback mechanism into the gradient update process. Meanwhile, a consensus-based ADMM is employed in [11] to derive the slope of the affine active power-reactive power (P-Q) rule, enabling the reactive power control strategy to adjust the reactive power of smart inverters based on an affine function of active power.

However, all these works are essentially based on first-order information, whose relatively slow convergence rates lead to poor tracking capabilities for time-varying environmental changes. Only a few studies utilize the second-order information to design VVC strategies. Reference [33] proposes an online hierarchical VVC scheme based on a projected-Newton method, which adopts a non-diagonal positive definite symmetric matrix developed from the Hessian matrix to scale the gradient and guarantee a fast convergence rate. In [34], a distributed quasi-Newton Broyden-Fletcher-Goldfarb-Shanno method is embedded into ADMM to generate an approximate Hessian matrix, thereby accelerating the convergence rate of the distributed VVC strategy. Nevertheless, both [33] and [34] impose relatively intensive computational burdens and costs in center or local agents, as the non-diagonal second-order information always hinders highly efficient distributed implementation and fast computational speed. Moreover, most of the studies do not take into account the influences of communication interruption during the online implementation, rendering them less robustness under non-ideal communication conditions.

To better address the rapid fluctuations in the operation of distribution networks, this paper proposes an online hierarchical VVC strategy for unbalanced distribution networks using diagonal-scaling ADMM (DS-ADMM), which is aimed at minimizing the voltage deviations and reactive power generation costs in time-varying environments. In contrast to the existing VVC strategies, the hierarchical VVC strategy further enhances the convergence performance via diagonal scaling skills and ensures robustness under under non-ideal communication conditions. It effectively addresses VVC optimization problem in time-varying environments. The main contributions of this paper are as follows.

1) The DS-ADMM is proposed to construct a diagonalized auxiliary matrix from the second-order Hessian matrix of the objective function. This construction enables DS-ADMM to leverage the acceleration properties of second-order information while maintaining scalability, thereby facilitating the online implementation of hierarchical VVC strategy.

2) The fast convergence rate of DS-ADMM is leveraged to enable the online implementation of hierarchical VVC strategy, thus effectively addressing the performance limitations of VCC strategy using ADMM in dynamic scenarios. Furthermore, the hierarchical VVC strategy is extended to unbalanced distribution networks, which enhances its applicability to practical distribution networks with inherent phase asymmetries.

3) A freezing strategy is considered in the hierarchical VVC strategy to improve its robustness, where previous measurement information is applied to make control decisions

under non-ideal communication conditions.

Finally, simulation studies on a modified IEEE 123-bus unbalanced distribution network are conducted to verify the effectiveness of the hierarchical VVC strategy using DS-ADMM and its robustness under non-ideal communication conditions. Its scalability is further demonstrated on the modified IEEE 8500-node test feeder.

II. VVC Optimization Problem Modeling

A. Model of Unbalanced Distribution Network

Consider an unbalanced radial distribution network with $N+1$ buses and set of unbalanced phases $\Phi=\{ph_a, ph_b, ph_c\}$. We set the set of bus indices as $\{0\}\bigcup\mathcal{N}$, where $\{0\}$ is the head bus of the distribution network; and $\mathcal{N}=\{1,2,\ldots,N\}$ is the set of all non-head buses. There are N line segments and each line segment can be single-phase, two-phase, or three-phase. For each bus $j\in\mathcal{N}$, let $b^p(j)\in\{0\}\bigcup\mathcal{N}$ denote the bus preceding bus j along the radial distribution network. Then, let $\mathcal{N}_j$ denote the set of all buses located strictly after bus j along the radial distribution network. Let $\mathcal{L}=\{\ell_j=(i,j)|i=b^p(j), j\in\mathcal{N}\}$ denote the set consisting of all distinct line segments $\ell_j=(i,j)$ in the distribution network. For each line segment, the model of the unbalanced linearized power flow [35] can be expressed as:

$$\boldsymbol{P}_{ij}=\sum_{m\in\mathcal{N}_j}\boldsymbol{P}_{jm}+\boldsymbol{p}_j \tag{1a}$$

$$\boldsymbol{Q}_{ij}=\sum_{m\in\mathcal{N}_j}\boldsymbol{Q}_{jm}+\boldsymbol{q}_j \tag{1b}$$

$$\boldsymbol{v}_i=\boldsymbol{v}_j+2(\bar{\boldsymbol{R}}_{ij}\boldsymbol{P}_{ij}+\bar{\boldsymbol{X}}_{ij}\boldsymbol{Q}_{ij}) \tag{1c}$$

$$\boldsymbol{a}_e=\left[1, \mathrm{e}^{-\mathrm{j}\frac{2\pi}{3}}, \mathrm{e}^{\mathrm{j}\frac{2\pi}{3}}\right]^{\mathrm{T}} \tag{1d}$$

$$\begin{cases}\bar{\boldsymbol{R}}_{ij}=\mathrm{Re}(\boldsymbol{a}_e\boldsymbol{a}_e^{\mathrm{H}})\odot\boldsymbol{R}_{ij}+\mathrm{Im}(\boldsymbol{a}_e\boldsymbol{a}_e^{\mathrm{H}})\odot\boldsymbol{X}_{ij}\\ \bar{\boldsymbol{X}}_{ij}=\mathrm{Re}(\boldsymbol{a}_e\boldsymbol{a}_e^{\mathrm{H}})\odot\boldsymbol{X}_{ij}-\mathrm{Im}(\boldsymbol{a}_e\boldsymbol{a}_e^{\mathrm{H}})\odot\boldsymbol{R}_{ij}\end{cases} \tag{1e}$$

where $\boldsymbol{R}_{ij}$ is the three-phase resistance matrix for line segment $\ell_j=(i,j)$; $\boldsymbol{X}_{ij}$ is the three-phase reactance matrix for line segment $\ell_j=(i,j)$; $\boldsymbol{a}_e^{\mathrm{H}}$ is the conjugate transpose of $\boldsymbol{a}_e$; Re(·) is the real part function; Im(·) is the imaginary part function; $\odot$ is the element-wise multiplicaiton operator; $\boldsymbol{P}_{ij}=[P_{ij}^{\phi}]$ and $\boldsymbol{Q}_{ij}=[Q_{ij}^{\phi}]$ are the matrices of three-phase active and reactive power flows for line segment $\ell_j=(i,j)$, respectively, P_{ij}^{ϕ} and Q_{ij}^{ϕ} are the active and reactive power flows for line segment $\ell_j=(i,j)$, respectively, and ϕ is the index of phases, $\phi\in\Phi$; $\boldsymbol{p}_j=[p_j^{\phi}]$ and $\boldsymbol{q}_j=[q_j^{\phi}]$ are the matrices of three-phase active and reactive loads at bus j, respectively, and p_j^{ϕ} and q_j^{ϕ} are the active and reactive loads at bus j, respectively; and $\boldsymbol{v}_j=[v_j^{\phi}]$ is the matrix of squared 3-phase voltage magnitudes at bus j, and v_j^{ϕ} is the squared voltage magnitude at bus j.

In (1), all terms are measured in per unit and ordered using the phase order ph_a, ph_b, and ph_c. The power flow (1) can be written as a compact matrix-vector form, which is given as:

$$\begin{cases}\boldsymbol{v}=-[\boldsymbol{A}^{\mathrm{T}}]^{-1}\boldsymbol{A}_0\boldsymbol{v}_0-2\boldsymbol{R}_D\boldsymbol{p}-2\boldsymbol{X}_D\boldsymbol{q}\\ \boldsymbol{R}_D=[\boldsymbol{A}^{\mathrm{T}}]^{-1}\boldsymbol{D}_r\boldsymbol{A}^{-1}\\ \boldsymbol{X}_D=[\boldsymbol{A}^{\mathrm{T}}]^{-1}\boldsymbol{D}_x\boldsymbol{A}^{-1}\end{cases} \tag{2}$$

where $\boldsymbol{D}_r=\mathrm{diag}(\bar{\boldsymbol{R}}_{b^p(1)1}, \bar{\boldsymbol{R}}_{b^p(1)2}, \ldots, \bar{\boldsymbol{R}}_{b^p(N)N})$ and $\boldsymbol{D}_x=\mathrm{diag}(\bar{\boldsymbol{X}}_{b^p(1)1}, \bar{\boldsymbol{X}}_{b^p(1)2}, \ldots, \bar{\boldsymbol{X}}_{b^p(N)N})$ are the block diagonal matrices of resistance and reactance, respectively, and $\bar{\boldsymbol{R}}_{b^p(N)N}$ and $\bar{\boldsymbol{X}}_{b^p(N)N}$ are the standard incidence matrices of $\boldsymbol{R}_{b^p(N)N}$ and $\boldsymbol{X}_{b^p(N)N}$, respectively; $\boldsymbol{p}=[\boldsymbol{p}_1,\boldsymbol{p}_2,\ldots,\boldsymbol{p}_N]^{\mathrm{T}}$ and $\boldsymbol{q}=[\boldsymbol{q}_1,\boldsymbol{q}_2,\ldots,\boldsymbol{q}_N]^{\mathrm{T}}$ are the net active and reactive power vectors, respectively; $\boldsymbol{A}$ is the connection structure between bus 0 and each of the line segments in $\mathcal{L}=\{\ell_j=(i,j)|i=b^p(j), j\in\mathcal{N}\}$; $\boldsymbol{A}_0$ is the connection structure between the remaining buses and each of the line segments in $\mathcal{L}=\{\ell_j=(i,j)|i=b^p(j), j\in\mathcal{N}\}$; and $\boldsymbol{v}_0$ is the voltage of bus 0.

Let $\boldsymbol{q}^g=[\boldsymbol{q}_1^g,\boldsymbol{q}_2^g,\ldots,\boldsymbol{q}_N^g]^{\mathrm{T}}$ and $\boldsymbol{q}^c=[\boldsymbol{q}_1^c,\boldsymbol{q}_2^c,\ldots,\boldsymbol{q}_N^c]^{\mathrm{T}}$ denote the vectors collecting the reactive power generation from DERs and the reactive power consumption, respectively, where $\boldsymbol{q}=\boldsymbol{q}^c-\boldsymbol{q}^g$. Substituting $\boldsymbol{q}=\boldsymbol{q}^c-\boldsymbol{q}^g$ into (2), we can obtain that:

$$\boldsymbol{v}=2\boldsymbol{X}_D\boldsymbol{q}^g-2\boldsymbol{X}_D\boldsymbol{q}^c-[\boldsymbol{A}^{\mathrm{T}}]^{-1}\boldsymbol{A}_0\boldsymbol{v}_0-2\boldsymbol{R}_D\boldsymbol{p} \tag{3}$$

Then, (3) can be written as:

$$\boldsymbol{v}=\boldsymbol{M}\boldsymbol{q}^g+\boldsymbol{\mu} \tag{4}$$

$$\boldsymbol{\mu}=-2\boldsymbol{X}_D\boldsymbol{q}^c-[\boldsymbol{A}^{\mathrm{T}}]^{-1}\boldsymbol{A}_0\boldsymbol{v}_0-2\boldsymbol{R}_D\boldsymbol{p} \tag{5}$$

where $\boldsymbol{M}=2\boldsymbol{X}_D$; and $\boldsymbol{\mu}$ is the uncontrollable variable vector.

B. Mathematical Formulation

The objective of hierarchical VVC strategy is to minimize voltage deviations and the reactive power generation costs of DERs, which can be formulated as:

$$\min f(\boldsymbol{v},\boldsymbol{q}^g)=\alpha x(\boldsymbol{v})+\beta y(\boldsymbol{q}^g)==\alpha\|\boldsymbol{v}-\boldsymbol{v}_r\|_2^2+\beta\|\boldsymbol{q}^g\|_{\boldsymbol{D}}^2 \tag{6a}$$

s.t.

$$\begin{cases}\underline{\boldsymbol{q}}^g\le\boldsymbol{q}^g\le\bar{\boldsymbol{q}}^g\\ \text{Eq. (2)}\end{cases} \tag{6b}$$

where $\boldsymbol{D}=\mathrm{diag}(d_1,d_2,\ldots,d_N)$ is the diagonal matrix, and d_N is the unit reactive power output cost of bus N; $\boldsymbol{v}_r=[v_{r1},v_{r2},\ldots,v_{rN}]$ is the reference vector of squared voltage magnitude, and v_{rN} is the reference value of squared voltage magnitude of bus N; $\underline{\boldsymbol{q}}^g=[\underline{\boldsymbol{q}}_1^g,\underline{\boldsymbol{q}}_2^g,\ldots,\underline{\boldsymbol{q}}_n^g]^{\mathrm{T}}$ and $\bar{\boldsymbol{q}}^g=[\bar{\boldsymbol{q}}_1^g,\bar{\boldsymbol{q}}_2^g,\ldots,\bar{\boldsymbol{q}}_n^g]^{\mathrm{T}}$ are the lower and upper var limits of $\boldsymbol{q}^g$, respectively; α and β are the weighting coefficients; $x(\boldsymbol{v})$ is the squared voltage deviation; and $y(\boldsymbol{q}^g)$ is the generation cost of reactive power.

III. Offline Implementation Framework for Hierachical VVC Strategy Using DS-ADMM

A. Overview

This subsection proposes a hierarchical VVC strategy using DS-ADMM to solve (6) in a distributed manner with fast convergence performance. In addition, an offline implementation framework for the hierarchical VVC strategy using DS-ADMM is designed in a static environment with a constant value of $\boldsymbol{\mu}$.

B. VVC Optimization Problem Reformulation

We introduce the auxiliary variable vector $\boldsymbol{z}=[z_1, z_2, \ldots, z_N]^{\mathrm{T}}$ such that $\boldsymbol{z}=\boldsymbol{q}^g$, where z_i is the auxiliary variable of bus i; thus, the VVC optimization problem (6) can be rewritten as:

$$\min g(\boldsymbol{q}^g)=\alpha\|\boldsymbol{M}\boldsymbol{q}^g+\boldsymbol{\mu}-\boldsymbol{v}_r\|_2^2+\beta\|\boldsymbol{q}^g\|_{\boldsymbol{D}}^2 \tag{7a}$$

s.t.

$$\underline{\boldsymbol{q}}^g\le\boldsymbol{z}\le\overline{\boldsymbol{q}}^g \tag{7b}$$

$$\boldsymbol{z}=\boldsymbol{q}^g \tag{7c}$$

where $g(\boldsymbol{q}^g)$ is the objective function.

Therefore, we define the set $\boldsymbol{Z}$ as:

$$\boldsymbol{Z}=\{\boldsymbol{z}|\underline{\boldsymbol{q}}^g\le\boldsymbol{z}\le\overline{\boldsymbol{q}}^g\} \tag{8}$$

Let $h(\boldsymbol{z})$ be the indicator function $I_z(\boldsymbol{z})$ for a closed convex set, as shown in (9).

$$h(\boldsymbol{z})=I_z(\boldsymbol{z})=\begin{cases}0 & \boldsymbol{z}\in\boldsymbol{Z}\\ +\infty & \boldsymbol{z}\notin\boldsymbol{Z}\end{cases} \tag{9}$$

The problem (7) is equivalently expressed as:

$$\min\{g(\boldsymbol{q}^g)+h(\boldsymbol{z})\} \tag{10a}$$

s.t.

$$\boldsymbol{z}=\boldsymbol{q}^g \tag{10b}$$

C. Hierarchical VVC Strategy Using DS-ADMM

Let $\boldsymbol{\gamma}=[\gamma_1, \gamma_2, \ldots, \gamma_N]^{\mathrm{T}}$ denote the dual variable vector associated with (10a), the augmented Lagrangian function L is given as:

$$L(\boldsymbol{q}^g,\boldsymbol{z},\boldsymbol{\gamma})=g(\boldsymbol{q}^g)+h(\boldsymbol{z})+\boldsymbol{\gamma}^{\mathrm{T}}(\boldsymbol{z}-\boldsymbol{q}^g)+\frac{\rho}{2}\|\boldsymbol{z}-\boldsymbol{q}^g\|^2 \tag{11}$$

where ρ is the augmented Lagrangian parameter.

With respect to (11), L can be directly solved by the ADMM in a distributed manner. The convergence performance of ADMM highly depends on the condition number of the VVC optimization problem κ, which can be given as:

$$\kappa=\frac{\lambda_{\max}(\alpha\boldsymbol{M}^{\mathrm{T}}\boldsymbol{M}+\beta\boldsymbol{D})}{\lambda_{\min}(\alpha\boldsymbol{M}^{\mathrm{T}}\boldsymbol{M}+\beta\boldsymbol{D})} \tag{12}$$

where $\lambda_{\max}(\alpha\boldsymbol{M}^{\mathrm{T}}\boldsymbol{M}+\beta\boldsymbol{D})$ and $\lambda_{\min}(\alpha\boldsymbol{M}^{\mathrm{T}}\boldsymbol{M}+\beta\boldsymbol{D})$ are the largest and smallest eigenvalues of $\alpha\boldsymbol{M}^{\mathrm{T}}\boldsymbol{M}+\beta\boldsymbol{D}$, respectively.

However, as the condition number of (7) can grow significantly with the increase in distribution network scale, the ADMM is faced with the slow convergence rate [36].

To enhance the convergence performance of ADMM for the VVC optimization problem, we propose to leverage the second-order information embedded in the problem. First, introduce a positive definite matrix $\boldsymbol{F}_i$ for local agent i (corresponds to bus i) and set $\boldsymbol{F}=blkdiag([\boldsymbol{F}_i]|i=1,2,\ldots,N)$, where *blkdiag* is the function to generate a matrix with given diagonal elements. Therefore, $\tilde{\boldsymbol{q}}^g$, $\tilde{\boldsymbol{z}}$, and $\tilde{\boldsymbol{\gamma}}$ can be given as:

$$\begin{cases}\tilde{\boldsymbol{q}}^g=\boldsymbol{F}\boldsymbol{q}^g\\ \tilde{\boldsymbol{z}}=\boldsymbol{F}\boldsymbol{z}\\ \tilde{\boldsymbol{\gamma}}=\boldsymbol{F}^{-1}\boldsymbol{\gamma}\end{cases} \tag{13}$$

The problem (10) can be equivalently reformulated as:

$$\min\{g(\boldsymbol{F}^{-1}\tilde{\boldsymbol{q}}^g)+h(\boldsymbol{F}^{-1}\tilde{\boldsymbol{z}})\} \tag{14a}$$

s.t.

$$\tilde{\boldsymbol{z}}=\tilde{\boldsymbol{q}}^g \tag{14b}$$

The augmented Lagrangian function for (14) is given as:

$$L(\tilde{\boldsymbol{q}}^g,\tilde{\boldsymbol{z}},\tilde{\boldsymbol{\gamma}})=g(\boldsymbol{F}^{-1}\tilde{\boldsymbol{q}}^g)+h(\boldsymbol{F}^{-1}\tilde{\boldsymbol{z}})+\tilde{\boldsymbol{\gamma}}^{\mathrm{T}}(\tilde{\boldsymbol{z}}-\tilde{\boldsymbol{q}}^g)+\frac{\rho}{2}\|\tilde{\boldsymbol{z}}-\tilde{\boldsymbol{q}}^g\|^2 \tag{15}$$

Next, define $\boldsymbol{B}_i$, $\boldsymbol{B}$, and $L_{\boldsymbol{B}}(\boldsymbol{q}^g,\boldsymbol{z},\boldsymbol{\gamma})$ as:

$$\boldsymbol{B}_i=\boldsymbol{F}_i^{\mathrm{T}}\boldsymbol{F}_i \tag{16a}$$

$$\boldsymbol{B}=\boldsymbol{F}^{\mathrm{T}}\boldsymbol{F} \tag{16b}$$

$$\begin{cases}L_{\boldsymbol{B}}(\boldsymbol{q}^g,\boldsymbol{z},\boldsymbol{\gamma})=L(\tilde{\boldsymbol{q}}^g,\tilde{\boldsymbol{z}},\tilde{\boldsymbol{\gamma}})=g(\boldsymbol{q}^g)+h(\boldsymbol{z})+\boldsymbol{\gamma}^{\mathrm{T}}(\boldsymbol{z}-\boldsymbol{q}^g)+\dfrac{\rho}{2}\|\boldsymbol{z}-\boldsymbol{q}^g\|_{\boldsymbol{B}}^2\\ \|\boldsymbol{z}-\boldsymbol{q}^g\|_{\boldsymbol{B}}^2=(\boldsymbol{z}-\boldsymbol{q}^g)^{\mathrm{T}}\boldsymbol{B}(\boldsymbol{z}-\boldsymbol{q}^g)\end{cases} \tag{16c}$$

Interestingly, the update processes of $\tilde{\boldsymbol{q}}^g$, $\tilde{\boldsymbol{z}}$, and $\tilde{\boldsymbol{\gamma}}$ can be equivalently expressed as the update processes of $\boldsymbol{q}^g$, $\boldsymbol{z}$, and $\boldsymbol{\gamma}$ by applying the ADMM to solve (14). The steps of update processes of $\tilde{\boldsymbol{q}}^g$, $\tilde{\boldsymbol{z}}$, and $\tilde{\boldsymbol{\gamma}}$ are given as follows.

Step 1: update $\boldsymbol{z}$.

$$\boldsymbol{z}^{(k+1)}=\arg\min_{\boldsymbol{z}\in\boldsymbol{Z}}L_{\boldsymbol{B}}((\boldsymbol{q}^g)^{(k)},\boldsymbol{z},\boldsymbol{\gamma}^{(k)})=\arg\min\{(\boldsymbol{\gamma}^{(k)})^{\mathrm{T}}\boldsymbol{z}+\rho/2(\boldsymbol{z}-(\boldsymbol{q}^g)^{(k)})^{\mathrm{T}}\boldsymbol{B}(\boldsymbol{z}-(\boldsymbol{q}^g)^{(k)})\} \tag{17}$$

where superscript (k) denotes the iteration number.

Step 2: update $\boldsymbol{q}^g$.

$$(\boldsymbol{q}^g)^{(k+1)}=\arg\min L_{\boldsymbol{B}}(\boldsymbol{q}^g,\boldsymbol{z}^{(k+1)},\boldsymbol{\gamma}^{(k)})=\arg\min\{g(\boldsymbol{q}^g)-(\boldsymbol{\gamma}^{(k)})^{\mathrm{T}}\boldsymbol{q}^g+\rho/2\|\boldsymbol{z}^{(k+1)}-\boldsymbol{q}^g\|_{\boldsymbol{B}}^2\} \tag{18}$$

Step 3: update $\boldsymbol{\gamma}$.

$$\boldsymbol{\gamma}^{(k+1)}=\boldsymbol{\gamma}^{(k)}+\rho\boldsymbol{\gamma}(\boldsymbol{z}^{(k+1)}-(\boldsymbol{q}^g)^{(k+1)}) \tag{19}$$

Remark: notably, two major challenges remain for the above implementation.

1) How to design $\boldsymbol{F}$ and $\boldsymbol{B}$ to facilitate the distributed implementation? It is still obscure how to perform the above steps in a distributed manner.

2) How to design $\boldsymbol{F}$ and $\boldsymbol{B}$ to optimally accelerate the convergence rate?

Fortunately, when $\boldsymbol{F}$ and $\boldsymbol{B}$ are designed as diagonal matrices, (17) can be distributionally performed by each local agent i as:

$$z_i^{(k+1)}=\arg\min L_{\boldsymbol{B}_i}((\boldsymbol{q}_i^g)^{(k)},z_i,\boldsymbol{\gamma}_i^{(k)})=\arg\min(\boldsymbol{\gamma}_i^{(k)})^{\mathrm{T}}z_i+\frac{\rho}{2}(z_i-(\boldsymbol{q}_i^g)^{(k)})^{\mathrm{T}}\boldsymbol{B}_i(z_i-(\boldsymbol{q}_i^g)^{(k)}) \tag{20}$$

In this case, (17)-(19) can be implemented in a hierarchical VVC strategy using DS-ADMM between the center agent and local agents, where the details of the hierarchical VVC strategy are given in Algorithm 1. The adaptation of diagonalized auxiliary matrices $\boldsymbol{F}$ and $\boldsymbol{B}$ can be interpreted by introducing the diagonal-scaling technology into the ADMM to form a DS-ADMM.

D. Determination of Diagonal Matrices

Let $\boldsymbol{H}$ to be the Hessian matrix of $g(\boldsymbol{q}^g)$ with respect to $\boldsymbol{q}^g$:

$$\boldsymbol{H}=\nabla^2 g(\boldsymbol{q}^g)=\alpha\nabla^2(\|\boldsymbol{M}\boldsymbol{q}^g+\boldsymbol{\mu}-\boldsymbol{v}_r\|)+\beta\nabla^2\|\boldsymbol{q}^g\|_{\boldsymbol{D}}^2=2(\alpha\boldsymbol{M}^{\mathrm{T}}\boldsymbol{M}+\beta\boldsymbol{D}) \tag{21}$$

Algorithm 1: DS-ADMM solution for (10)

Initialization: set $k=0$, $(\boldsymbol{q}_i^g)^{(0)}$, $\boldsymbol{z}^{(0)}$, $\boldsymbol{\gamma}^{(0)}$, center agent estimates $\boldsymbol{\mu}$ corresponding to initial state of system by (5), and each local agent i sends $\boldsymbol{F}_i$ and $\boldsymbol{B}_i$ to center agent.

For $k \geq 0$: follow *Steps 1-4* of the ADMM, alternately updating the variables until convergence.

Step 1: update $\boldsymbol{z}$ using (17). Each local agent i updates and sends $\boldsymbol{z}_i^{(k)}$ to center agent.

Step 2: update $\boldsymbol{q}^g$ using (18). $(\boldsymbol{q}_i^g)^{(k+1)}$ is updated by the center agent.

Step 3: update $\boldsymbol{\gamma}$ using (19). Center agent communicates $(\boldsymbol{q}^g)^{(k+1)}$ and $\boldsymbol{\gamma}^{(k+1)}$ to local agent i. $\boldsymbol{\gamma}^{(k+1)}$ can also be updated by local agent i.

Step 4: update number of iterations until $k > k_{\max}$, where $k_{\max}$ is the maximum iteration.

It is proven in [37] that the convergence rate is faster for a smaller ratio $\lambda_{\max}(\boldsymbol{F}^{-\mathrm{T}}\boldsymbol{H}\boldsymbol{F}^{-1})/\lambda_{\min}(\boldsymbol{F}^{-\mathrm{T}}\boldsymbol{H}\boldsymbol{F}^{-1})$, where $\lambda_{\max}(\boldsymbol{F}^{-\mathrm{T}}\boldsymbol{H}\boldsymbol{F}^{-1})$ and $\lambda_{\min}(\boldsymbol{F}^{-\mathrm{T}}\boldsymbol{H}\boldsymbol{F}^{-1})$ are the maximum and minimum eigenvalues of $\boldsymbol{F}^{-\mathrm{T}}\boldsymbol{H}\boldsymbol{F}^{-1}$, respectively. In addition, to facilitate the distributed hierarchical implementation of VVC, it is required to construct $\boldsymbol{F}$ as a diagonal matrix. That is, we aim to find a diagonal matrix $\boldsymbol{F}$ to minimize the ratio $\lambda_{\max}(\boldsymbol{F}^{-\mathrm{T}}\boldsymbol{H}\boldsymbol{F}^{-1})/\lambda_{\min}(\boldsymbol{F}^{-\mathrm{T}}\boldsymbol{H}\boldsymbol{F}^{-1})$, thus accelerating the convergence rate while ensuring the distributed hierarchical implementation as follows.

$$\min_{\boldsymbol{F}} \frac{\lambda_{\max}(\boldsymbol{F}^{-\mathrm{T}}\boldsymbol{H}\boldsymbol{F}^{-1})}{\lambda_{\min}(\boldsymbol{F}^{-\mathrm{T}}\boldsymbol{H}\boldsymbol{F}^{-1})} \tag{22}$$

It is proved in [36] that (22) can be equivalently solved by the following semi-definite convex program.

$$\min_{t,\boldsymbol{B}} t \tag{23a}$$

s.t.

$$t\boldsymbol{H} \succcurlyeq \boldsymbol{B} \tag{23b}$$

$$\boldsymbol{B} \succcurlyeq \boldsymbol{H} \tag{23c}$$

where $\boldsymbol{B}$ is a diagonal matrix; and t is the time.

From $\boldsymbol{B}=\boldsymbol{F}^{\mathrm{T}}\boldsymbol{F}$, we can obtain a diagonal positive definite matrix $\boldsymbol{F}$ that minimizes the ratio of the maximum eigenvalue to the minimum eigenvalue of $\boldsymbol{F}^{-\mathrm{T}}\boldsymbol{H}\boldsymbol{F}^{-1}$.

IV. Online Implementation Framework for Hierachical VVC Strategy Using DS-ADMM

A. Overview

The offline implementation framework considers a constant external environment, where the uncontrollable variable $\boldsymbol{\mu}$ is treated as a constant value in (5). However, the environmental changes are time-varying in the real world, resulting in dynamic fluctuations in the distribution network. These dynamic fluctuations are reflected in the time-varying $\boldsymbol{\mu}$. As the rate of time-varying environmental changes is faster than the convergence rate, the external environment may have changed before implementing the optimal solution determined by the offline implementation framework. To address this challenge, the online implementation framework is proposed, which corresponds to the online hierarchical VVC strategy using DS-ADMM. Figure 1 shows the process of the online implementation framework, which means the process of online hierarchical VVC strategy. As shown in Fig. 1, each local agent i directly performs and updates its decisions, i.e., the reactive power output of local PV inverter, after each iteration without any need to wait for the DS-ADMM convergence, thus enabling a timely response to the time-varying environmental changes. Furthermore, the DS-ADMM is introduced to enhance the performance of the hierarchical VVC strategy to track the time-varying environmental changes, leveraging its superior convergence rate.

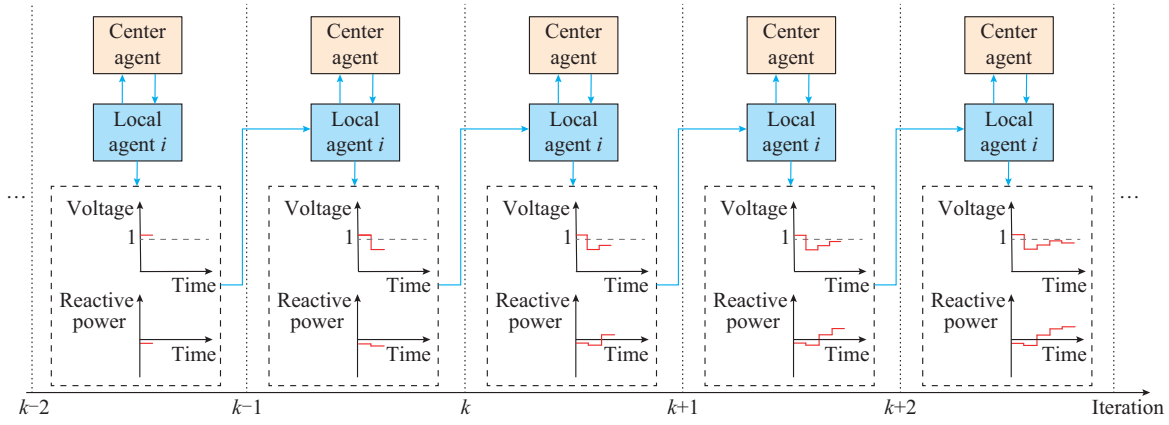

Fig. 1. Process of online implementation framework.

B. Online Implementation Framework

In the offline implementation framework, the goal is to solve the problem (7), where $\boldsymbol{\mu}$ is assumed to be constant. In addition, it can be observed from (4) that $\boldsymbol{\mu}$ is approximately calculated based on the linearized distribution power flow in the offline implementation framework, leaving two major challenges.

1) The linearized distribution power flow fails to consider the nonlinear characteristics of power flow, thereby compromising the solution accuracy to some extent.

2) The value of $\boldsymbol{\mu}$ can only change after Algorithm 1 is converged in the offline implementation framework, but the fast time-varying environmental changes may lead to the change of $\boldsymbol{\mu}$ before Algorithm 1 is converged.

In contrast, the online implementation framework resolves the above two major challenges as follows.

1) Instead of updating $\boldsymbol{\mu}$ by (4), we update $\boldsymbol{\mu}^{(k)}$ based on the real-time voltage measurement $\hat{\boldsymbol{v}}^{(k)}$ at each iteration k.

$$\boldsymbol{\mu}^{(k)} = \hat{\boldsymbol{v}}^{(k)} - \boldsymbol{M}(\boldsymbol{q}^{g})^{(k)} \tag{24}$$

The key feature of the online implementation framework is its own closed-loop nature, which utilizes the most up-to-date voltage measurements to estimate $\boldsymbol{\mu}^{(k)}$. Such an update manner accounts for the nonlinear characteristics of the power flow.

2) The online implementation framework directly performs its decision after each iteration without the need to wait for the convergence. The fast time-varying environmental changes are inherently reflected and captured by the real-time voltage measurements $\hat{\boldsymbol{v}}^{(k)}$, thus affecting the value of $\boldsymbol{\mu}^{(k)}$. The change of $\boldsymbol{\mu}^{(k)}$ may further change the decision making at each iteration k. By updating $\boldsymbol{\mu}^{(k)}$, the online implementation framework enables the real-time tracking of the environmental changes.

The steps of the online implementation framework is outlined as follows.

Step 1: local agent i measures and updates the real-time voltage magnitude $\hat{\boldsymbol{v}}^{(k)}$.

Step 2: local agent i updates auxiliary variable $\boldsymbol{z}_i^{(k)}$ and uploads $\hat{\boldsymbol{v}}^{(k)}$ and $\boldsymbol{z}_i^{(k)}$ to the center agent.

Step 3: center agent receives data from all local agents and aggregates them to get $\hat{\boldsymbol{v}}^{(k)}$ and $\boldsymbol{z}^{(k)}$, then calculates $\boldsymbol{\mu}^{(k)}$ based on (24).

Step 4: center agent performs updating of $(\boldsymbol{q}^{g})^{(k)}$ and $\boldsymbol{\gamma}^{(k)}$ and communicates $(\boldsymbol{q}_i^{g})^{(k)}$ and $\boldsymbol{\gamma}_i^{(k)}$ to the corresponding local agent i.

Step 5: local agent i adjusts reactive power output of PV inverter connected to bus i according to received $(\boldsymbol{q}_i^{g})^{(k)}$.

By executing *Steps 1-5* in each iteration, the hierarchical VVC strategy updates control decisions in real time, thus effectively tracking the time-varying environmental changes.

C. Considering Non-ideal Communication Condition

Section IV-B assumes ideal communication conditions, but there are a series of communication issues in the real world, e.g., random delays and packet loss [24]. This subsection focuses on further enhancing the robustness of online implementation framework under non-ideal communication conditions.

To this end, we propose a freezing strategy characterized by quasi-asynchronous updates. This freezing strategy eliminates the need to wait for the completion of all data transmissions before performing calculations. Instead, the data from the previous iteration are frozen and are used to replace any corresponding data that can not be received within the specified communication time, ensuring the smooth execution of the current iteration. Figure 2 shows the iteration process under non-ideal communication condition. Consider three different local agents i, j, and n, where local agent i is a normal agent without any communication failure; and local agents j and n are agents with information transmission failure and reception failure, respectively. In Fig. 2, the dashed box represents data stored after iteration k; and the solid box represents data updated after iteration $k+1$. For the center agent, the data transmission step involves only the local voltage measurements and auxiliary variables of local agents i and n. The local voltage measurements and auxiliary variables of agent j are kept the same as the previous iteration due to its information transmission failure. After the date update, the center agent may calculate $(\boldsymbol{q}_i^{g})^{(k+1)}$, $(\boldsymbol{q}_j^{g})^{(k+1)}$, $(\boldsymbol{q}_n^{g})^{(k+1)}$, $\boldsymbol{\gamma}_i^{(k+1)}$, $\boldsymbol{\gamma}_j^{(k+1)}$, and $\boldsymbol{\gamma}_n^{(k+1)}$, and send them to local agents i, j, and n. Given the information reception failure of local agent n, the local agent n may directly perform $\boldsymbol{q}_n^{g}(k)$ instead of $(\boldsymbol{q}_n^{g})^{(k+1)}$, as it fails to receive $(\boldsymbol{q}_i^{g})^{(k+1)}$ and $\boldsymbol{\gamma}_n^{(k+1)}$ from the center agent at iteration $k+1$. The above steps construct an approximate asynchronous iteration process, which effectively mitigates the impact of communication failures in online implementation framework. The robustness of the hierarchical VVC strategy using DS-ADMM will be validated in Section V.

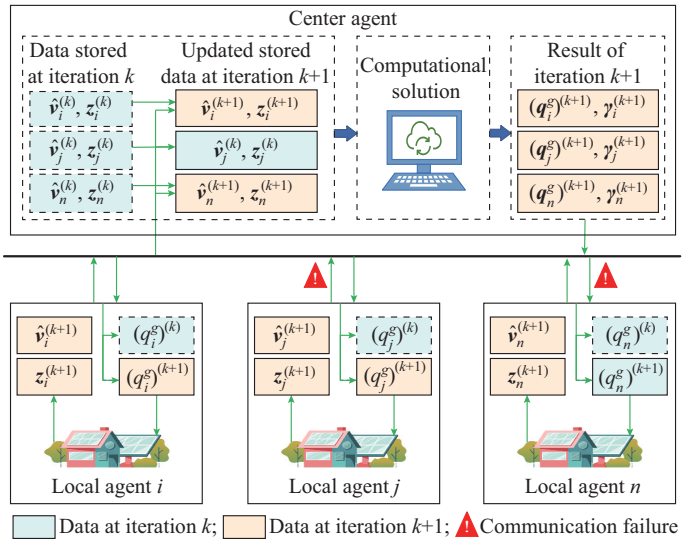

Fig. 2. Iteration process under non-ideal communication condition.

It is worth noting that, in the following content, the hierarchical VVC strategy using DS-ADMM is short for the proposed strategy.

V. Numerical Case Study

A. Overview

A modified IEEE 123-bus unbalanced distribution network is considered to demonstrate the effectiveness of the proposed strategy, as shown in Fig. 3. The base power and voltage are set to be $S_{\text{base}} = 100$ kVA and $V_{\text{base}} = 4.16$ kV, respectively. The squared voltage magnitude for bus 0 is set to be $v_0 = 1$ p.u. and the reference of squared voltage magnitude is set to be $\boldsymbol{v}_r = [1, 1, \ldots, 1]$, $\boldsymbol{D} = \boldsymbol{1}_{n\times n}$ (which is a $n \times n$ identity matrix), $\boldsymbol{v}_{\min} = [0.95^2, 0.95^2, \ldots, 0.95^2]$, and $\boldsymbol{v}_{\max} = [0.95^2, 0.95^2, \ldots, 0.95^2]$. PV inverters are distributed across the distribution network, as shown in Fig. 3, with the reactive power limits $\underline{\boldsymbol{q}}_i^{g} = -0.1$ p.u. and $\overline{\boldsymbol{q}}_i^{g} = 0.1$ p.u.. The augmented Lagrangian parameter is set to be $\rho = 20$, and the weighting co-

efficients are chosen as $\alpha=4$ and $\beta=0.5$.

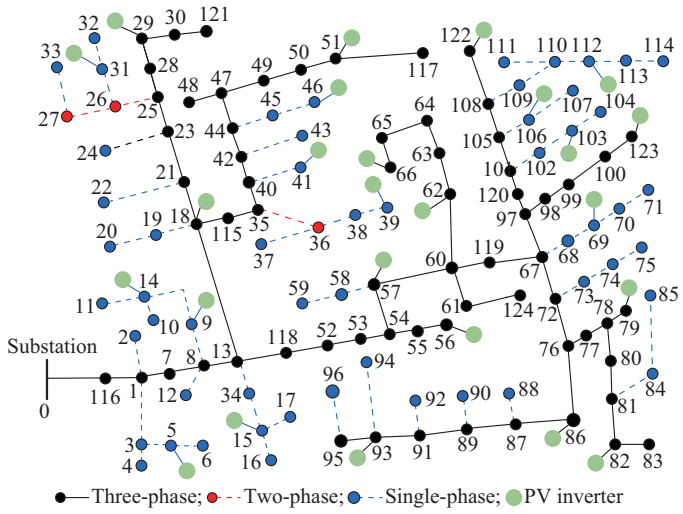

Fig. 3. Modified IEEE 123-bus unbalanced distribution network.

Static and dynamic scenarios are both considered in the numerical case study. In the static scenario, we assume that the unbalanced load remains constant, with 24 sets of unbalanced load data representing the load profile throughout a 24-hour period. Figure 4 shows the aggregate load and PV generation throughout a 24-hour period. The dynamic scenario considers minute-level real-time load variations.

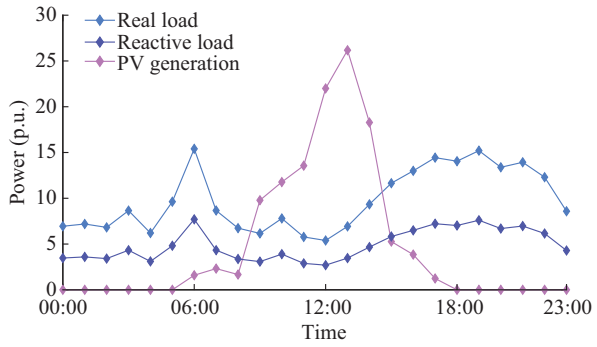

Fig. 4. Aggregate load and PV generation throughout 24-hour period.

In the numerical case study, Sections V-B and V-C present the results of the proposed strategy under the offline implement framework, while the remaining subsections present the results of the proposed strategy under the online implement framework.

B. Static Scenario

In this subsection, we validate the effectiveness of the proposed strategy under the static scenario. To better demonstrate the applicability of the proposed strategy, the static scenario includes high-load and low-PV conditions (e. g, profiles at 06:00), and high-PV and low-load conditions (e. g., profiles at 12:00 and 13:00). The case study simulates voltage profiles throughout a 24-hour period, comparing the performance with and without the proposed strategy.

Figure 5 shows the maximum and minimum voltage magnitudes for each phase of the distribution network. From the simulation results shown in Fig. 5, it can be observed that there are voltage violations across all three phases of the distribution network, particularly in phases a and c without the proposed strategy. The maximum voltage exceeds 1.06 p. u., and the minimum voltage falls below 0.94 p. u., both of which are unacceptable for the safe operation of distribution network. In contrast, with the proposed strategy, voltage levels across the distribution network remain within the safe range throughout the 24-hour period.

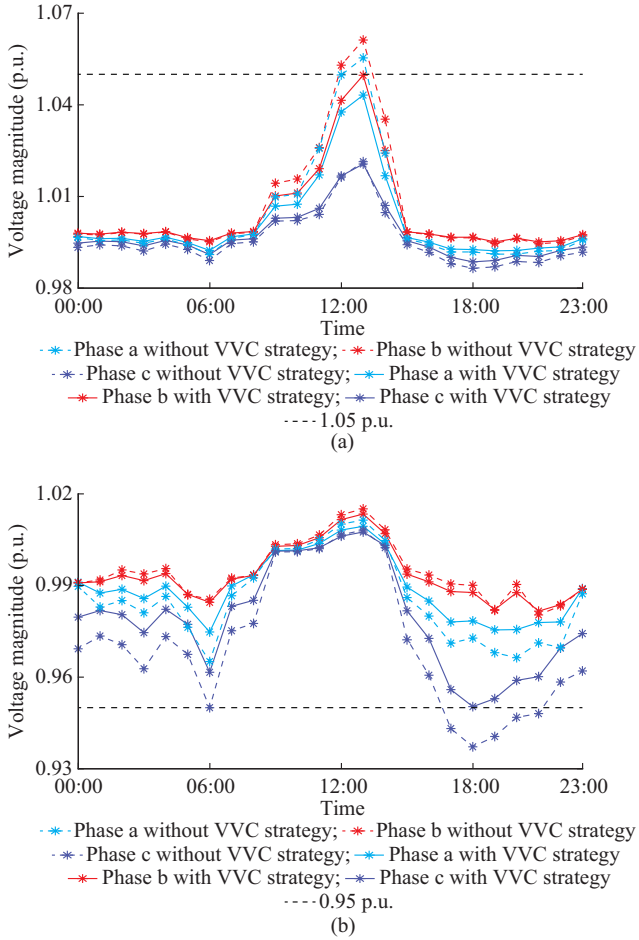

Fig. 5. The maximum and minimum voltage magnitudes for each phase of distribution network. (a) The maximum voltage magnitude. (b) The minimum voltage magnitude.

C. Performance Comparisons

To demonstrate the optimality of DS-ADMM, we introduce several representative VVC strategies for comparison, which are given as follows.

Strategy 1: centralized VVC strategy. Directly solve the VVC optimization problem based on centralized optimization.

Strategy 2: hierarchical VVC strategy using ADMM [28]. Directly solve the VVC optimization problem based on the ADMM.

Strategy 3: local delayed droop control (DDC) -based VVC strategy [19]. Each local agent independently performs its own voltage control based on its local V-Q curve.

Strategy 4: the proposed strategy (hierarchical VVC strate-

gy using DS-ADMM).

Using the results of centralized optimization as a benchmark, the voltage magnitudes of each bus in modified IEEE 123-bus unbalanced distribution network at 17:00 under four strategies are shown in Fig. 6. The results of strategies 2 and 4 perfectly match the centralized optimization results. However, the result of strategy 3 fails. In addition, the result of strategy 3 shows an obvious under-voltage issue for phase c.

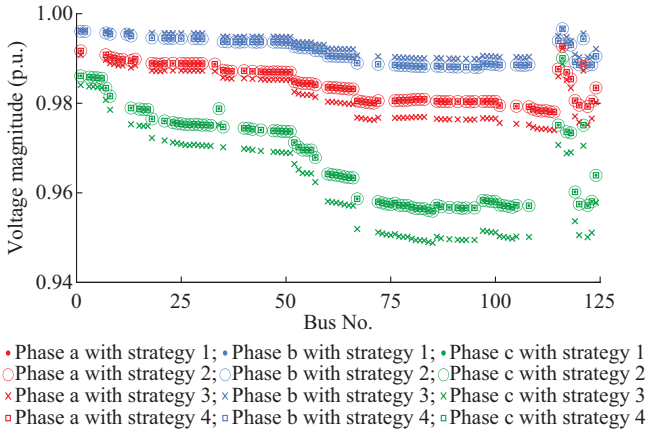

Fig. 6. Voltage magnitudes of each bus in modified IEEE 123-bus unbalanced distribution network at 17:00 under four strategies.

Subsequently, we compare the convergence performance of the ADMM, DS-ADMM, DDC, and centralized optimization algorithms. Taking bus 93 at 17:00 as an example, the reactive power outputs of phases a, b, and c and the voltages of PV inverters are depicted in Figs. 7 and 8, respectively.

The simulation results clearly demonstrate that DS-ADMM converges significantly faster than the ADMM. For the ADMM, the reactive power of PV inverter converges after around 80 iterations, and its voltage profile takes at least 50 iterations to converge. But for the proposed strategy, it achieves the convergence for all results in about 20 iterations and also reaches the optimal solution of centralized optimization. The DDC lacks the capability of converging the optimal solution. The above results demonstrate that the proposed strategy not only ensures optimality but also exhibits excellent convergence performance. Such characteristics facilitate the online implementation framework to track the time-varying environments.

To further validate the effectiveness and superiority of the proposed strategy, a comparative analysis is conducted among centralized optimization, DDC, ADMM, and DS-ADMM under different step-size settings. The convergence criterion is defined as the reactive power difference between two consecutive iterations being less than a specified tolerance δ, $|(\boldsymbol{q}^g)^{(k)} - (\boldsymbol{q}^g)^{(k-1)}| < \delta$, where δ is set to be 0.0001. Table I summarizes the comparison of performances of different algorithms in terms of the voltage deviation, reactive power generation costs from DERs, the objective value, and convergence speed (measured by both iterations and total computation time). The DS-ADMM consistently achieves faster convergence than ADMM across all different step sizes, while maintaining performance close to that of the centralized optimization.

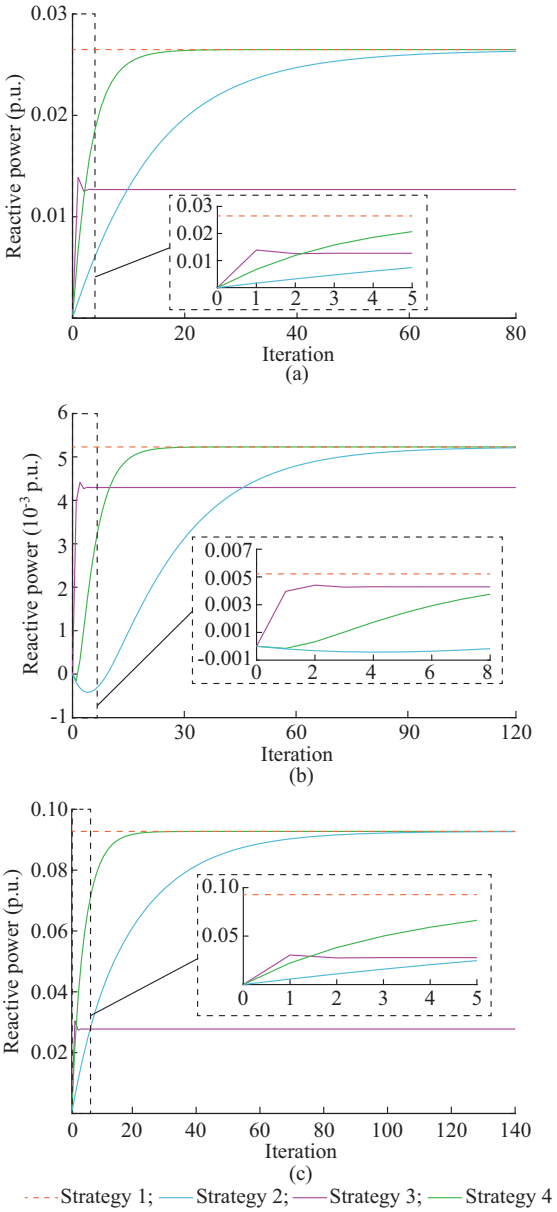

Fig. 7. Comparison of reactive power outputs of PV inverters at bus 93 at 17:00. (a) Phase a. (b) Phase b. (c) Phase c.

Although DDC yields lower reactive power costs, it fails to provide sufficient reactive power support from PV inverters, leading to poor voltage control performance. Overall, the results indicate that DS-ADMM offers a favorable trade-off between convergence speed and optimality.

D. Dynamic Scenario

This subsection validates and verifies the performance of the proposed strategy in the dynamic scenarios. Since centralized optimization is not feasible for online VVC, we conduct experiments in dynamic scenarios using strategies 2-4. Using the load at 18:00 as the baseline, load change rates ranging from 10% to 90% are used to evaluate and compare the control performances of strategies 2-4 under time-varying environmental changes (correspond to different load change rates). The cumulative errors of strategies 2-4 with 10, 20, and 30 iterations under different load change rates are shown in Fig. 9.

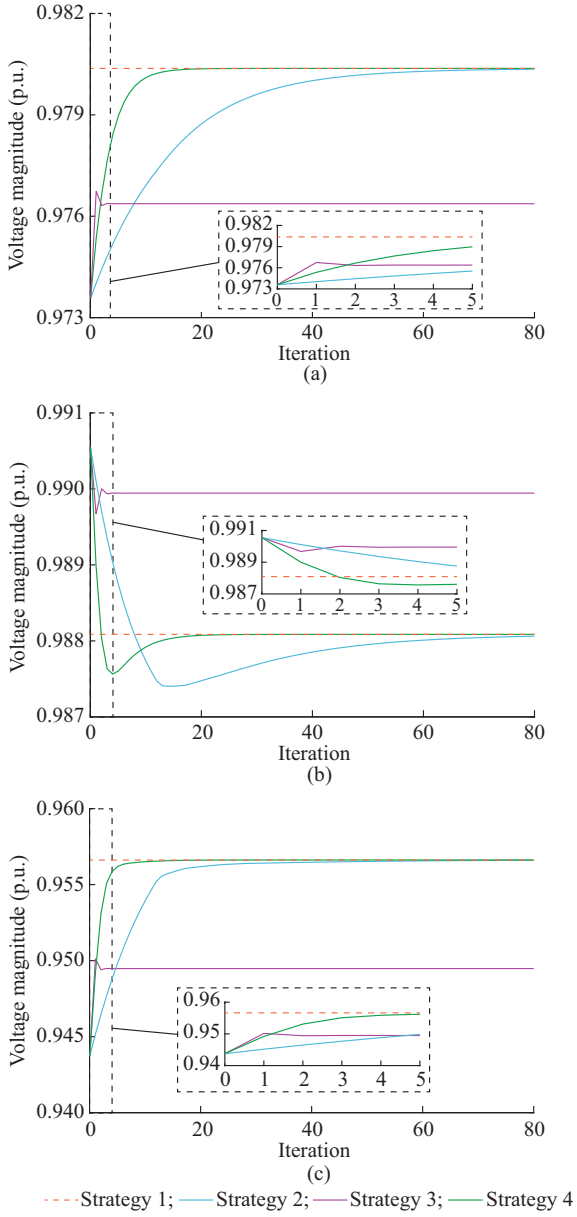

Fig. 8. Comparison of voltages of PV inverters at bus 93 at 17:00. (a) Phase a. (b) Phase b. (c) Phase c.

TABLE I
COMPARISON OF PPERFORMANCES OF DIFFERENT ALGORITHMS

Algorithm	Step size	$x(\boldsymbol{v})$	$y(\boldsymbol{q}^g)$	$f(\boldsymbol{v},\boldsymbol{q}^g)$	Convergence iteration count	Computational time (s)
Centralized optimization		0.53264	0.10264	2.18189		
DDC		0.71193	0.01853	2.85710	5	0.40
ADMM	10	0.53300	0.10228	2.18316	47	9.28
	20	0.53365	0.10165	2.18541	76	16.30
	40	0.53503	0.10030	0.19026	123	30.56
DS-ADMM	10	0.53258	0.10271	2.18167	16	3.00
	20	0.53267	0.10261	2.18120	25	4.53
	40	0.53290	0.10239	2.18279	40	7.33

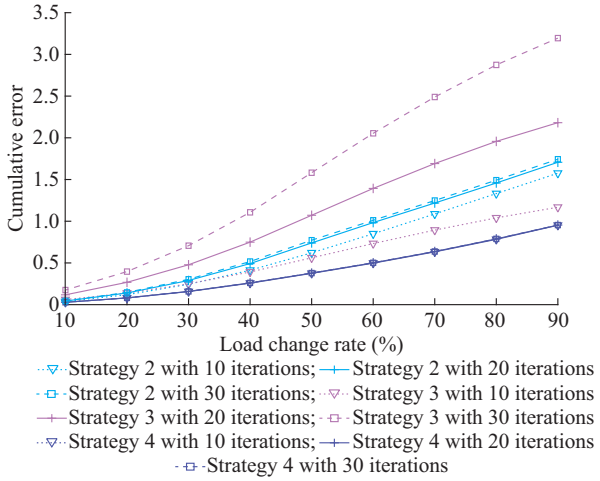

Fig. 9 Cumulative errors of strategies 2, 3, and 4 with 10, 20, and 30 iterations under different load change rates.

The vertical axis represents the cumulative error of the objective function relative to the baseline throughout the iteration process. As shown in Fig. 9, the cumulative error of strategy 3 is larger than that of strategy 2 and strategy 4 with 10 iterations. However, with 20 and 30 iterations, the cumulative errors of strategy 3 become more similar and are both smaller than the cumulative error of strategy 2. This is because although DDC converges much faster than ADMM, it is unable to reach the optimal value, causing the cumulative error to increase significantly as the number of iterations grows.

In contrast, strategy 4 shows highly overlapping cumulative error curves from 10 to 30 iterations and consistently produces lower cumulative errors compared to other strategies. This indicates that DS-ADMM has a significant advantage in terms of convergence speed and optimality. These results further highlight the superior applicability of strategy 4 in time-varying environments.

The proposed strategy is further verified in continuous fast time-varying environments. The actual minute-level PV output and customer load data are applied to simulate the fast time-varying environmental changes, and the aggregate load and PV generation under continuous fast time-varying environmental changes are depicted in Fig. 10. In the online framework, the time interval of each iteration is set to be 5 s.

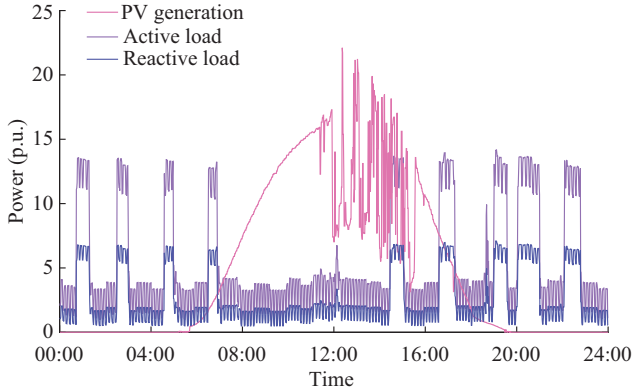

Fig. 10. Aggregate load and PV generation under continuous fast time-varying environmental changes.

Figure 11 illustrates the voltage distribution of the modified IEEE 123-bus unbalanced distribution network over a 24-hour period with strategies 2-4, where the orange and blue dashed lines represent the voltage limits, 0.95 p.u. and 1.05 p.u., respectively. The system voltage drops below 0.94 p.u. at its lowest and rises to nearly 1.06 p.u. at its highest in the absence of the VVC strategy. After implementing various VVC strategies, only strategy 4 ensures that the voltage remains within the safe range throughout the 24-hour period.

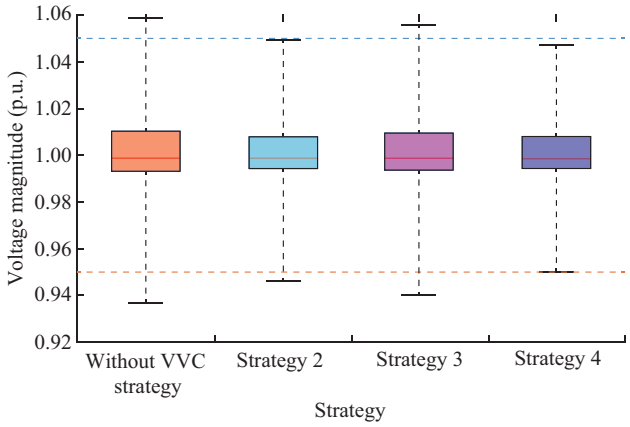

Fig. 11. Voltage distribution of modified IEEE 123-bus unbalanced distribution network over 24-hour period with strategies 2-4.

Figure 12 illustrates the reactive power output of the PV inverter connected to phase a at bus 57 between 13:00 and 14:00. We assume that the changes in the environment are known a priori in each iteration time window and consider the results under the corresponding offline problem solved by centralized optimization as a benchmark. Although the fast time-varying environmental changes make this unachievable in practice, strategy 4 shows the best performance to compare with other strategies.

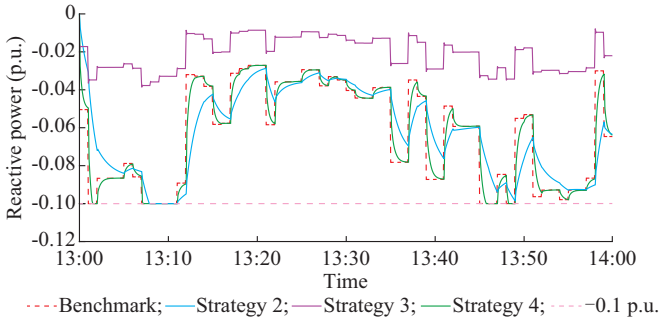

Fig. 12. Reactive power output of PV inverter connected to phase a at bus 57 between 13:00 and 14:00.

Specifically, strategy 2 exhibits a significant deviation between its own reactive power decision and its optimal value. Strategy 3 exhibits insufficient algorithm convergence when there are drastic load fluctuations, leading to a longer adjustment time for the inverter to reach the optimal reactive output. In contrast, strategy 4 can quickly respond to fast time-varying environmental changes, allowing the PV inverter to reach the optimal output in a shorter time. The above results demonstrate that strategy 4 shows a stronger capability of harnessing the reactive power of the PV inverter, thereby ensuring more excellent voltage control performance.

With the penetration of PV systems, the proposed strategy is able to exploit the reactive power regulation potential of PV inverters more efficiently, which not only reduces the need for the configuration of specialized reactive power regulation equipment, such as capacitors and static reactive power generators (SVGs), but also ensures that the distribution network voltage always operates within a safe range.

E. Algorithm Scalability: IEEE 8500-node Test Feeder

To test the scalability of the proposed strategy, we modify the IEEE 8500-node test feeder by adding several 100 kVA PV inverters, as shown in Fig. 13. The base voltage is set to be 7.2 kV, and the base power is set to be 100 kVA. Figure 14 illustrates the aggregate load and PV generation throughout a 60 min simulation period.

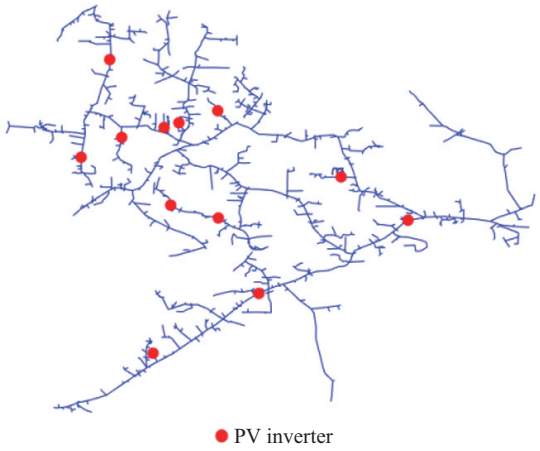

Fig. 13. Modified IEEE 8500-node test feeder.

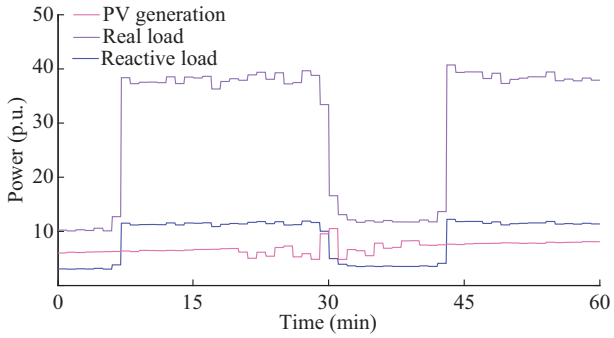

Fig. 14. Aggregate load and PV generation throughout 60 min simulation period.

Figure 15 presents the minimum voltage distribution in modified IEEE 8500-node test feeder. It can be observed that the proposed strategy effectively mitigates voltage violations in a large unbalanced distribution network.

Figure 16 shows the voltage distribution of the modified IEEE 8500-node test feeder with and without different VVC strategies over a one-hour period. It can be observed that only the proposed strategy successfully avoids voltage violations, demonstrating its scalability in large distribution networks. In contrast, the maximum voltage under strategies 2

and 3 is slightly higher than that without VVC strategy. This is mainly because strategy 3 adjusts inverter outputs based solely on local node conditions, without awareness of the system-wide voltage performance. Furthermore, strategy 3 suffers from the limited convergence speed of the ADMM algorithm, leading to poor responsiveness to rapid fluctuations.

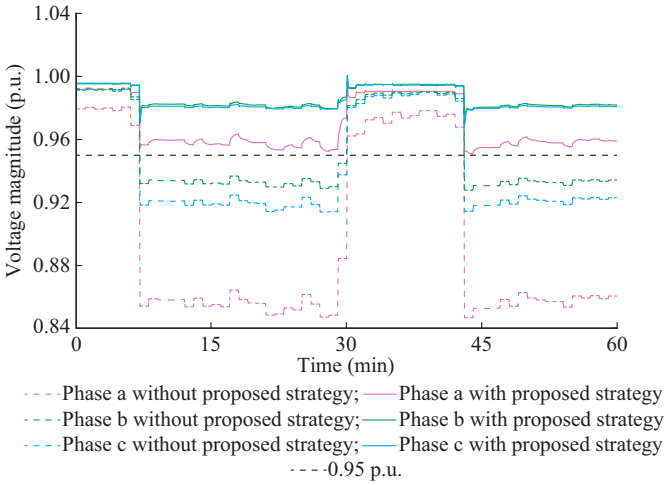

Fig. 15. The minimum voltage magnitude in modified IEEE 8500-node test feeder.

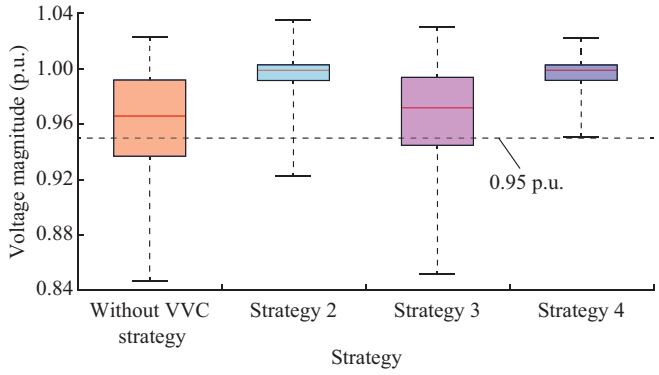

Fig. 16. Voltage distribution of modified IEEE 8500-node test feeder with and without different VVC strategies.

F. Robustness Verification

This subsection considers the freezing strategy, depicted in Section IV, to validate the robustness of the online proposed strategy under non-ideal communication conditions. We assume that communication interruptions, e.g., packet loss, occur randomly during interactions between local agents and the center agent, and define following communication environment:

Case 1: ideal communication.

Case 2: 10% random communication failures.

Case 3: 30% random communication failures.

Case 4: 50% random communication failures.

First, we conduct 3 sets of experiments with communication failure rates ranging from 10% to 30%. For each set, we run 10 simulations for both ADMM and DS-ADMM, and compare the average number of iterations required for the algorithm convergence. Here, we still set $\delta = 0.0001$. The results are shown in Table II. As seen in Table II, although the number of iterations required for convergence increases for both ADMM and DS-ADMM as the communication failure rate increases, the increase for DS-ADMM is much smaller than that for ADMM. Even under most non-ideal communication conditions, DS-ADMM exhibits better convergence performance than ADMM under ideal conditions.

TABLE II
AVERAGE NUMBER OF ITERATIONS FOR DIFFERENT ALGORITHMS UNDER VARIOUS COMMUNICATION FAILURE RATES

Case No.	Number of iterations	
	ADMM	DS-ADMM
1	78.0	25.0
2	105.6	30.7
3	129.5	40.1
4	170.9	49.1

Next, using the same baseline values as in the Section V-D, we compare the cumulative errors between 13:00 and 14:00 for the online implementation of strategies 3 and 4 across the communication environments of cases 1-4, as shown in Fig. 17. It can be observed that the cumulative error increases for both strategy 3 and strategy 4 as the communication environment changes. However, the cumulative error of strategy 4 in case 4 increases by only 11.5% compares to than in Case 1, while the cumulative error of strategy 3 increases by 21%. In particular, even in the worst communication environment, the cumulative error of strategy 4 remains significantly lower than that of strategy 3 in the ideal communication environment. These results clearly highlight the superior robustness of DS-ADMM in imperfect communication environments.

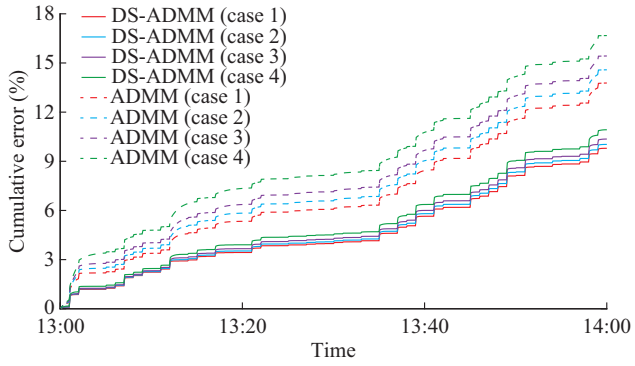

Fig. 17. Cumulative errors between 13:00 and 14:00 for VVC strategy in communication environment.

VI. CONCLUSION

In this paper, the online hierarchical VVC strategy using DS-ADMM for unbalanced distribution networks is proposed to coordinate the reactive power output of PVs in real time through online interaction between the local agents and center agent. By diagonalizing the second-order Hessian matrix of the objective function, a DS-ADMM with excellent convergence rate for distributed computing is proposed. Compared with existing ADMM-based and hierarchical VVC strategies, the proposed strategy using DS-ADMM sig-

nificantly improves the tracking ability in the time-varying environment.

Numerical case studies validate the effectiveness of the proposed strategy in both static and dynamic scenarios. Comparisons with the local DDC-based VVC strategy and the ADMM-based hierarchical strategy show that the propsed strategy achieves better performance in terms of convergence, optimality, and scalability. It converges more quickly in static conditions and tracks time-varying environmental changes more effectively in dynamic environments. Additionally, it performs well even in non-ideal communication environments.

Future research will focus on two directions.

1) Computationally efficient VVC for large-scale distribution systems: we will develop optimized voltage control strategies that minimize computational and communication burdens through intelligent selection of key regulatory nodes and implementation of asynchronous communication protocols.

2) Fully distributed VVC architecture: we will create a novel online control framework based on DS-ADMM that eliminates centralized dependencies. This peer-to-peer approach enables direct neighbor-to-neighbor coordination, which is inherently robust against single-point failures while maintaining system-wide voltage stability.

REFERENCES

[1] J. Blanes, F. Toledo, S. Montero *et al*., "In-site real-time photovoltaic *I-V* curves and maximum power point estimator," *IEEE Transactions on Power Electronics*, vol. 28, no. 3, pp. 1234-1240, Mar. 2013.

[2] SolarTech Lab Test Facility. (2020, Oct.). Solar desalination system. [Online]. Available: http://www.solartech.polimi.it/

[3] Y. Wang, K. Tan, X. Peng *et al*., "Coordinated control of distributed energy-storage systems for voltage regulation in distribution networks," *IEEE Transactions on Power Delivery*, vol. 31, no. 3, pp. 1132-1141, Jun. 2016.

[4] M. R. Dar and S. Ganguly, "Dual-stage model predictive control based reduced model framework for voltage control in active distribution networks," *Journal of Modern Power Systems and Clean Energy*, vol. 12, no. 6, pp. 1880-1892, Nov. 2024.

[5] H. Pezeshki, A. Arefi, G. Ledwich *et al*., "Probabilistic voltage management using OLTC and dSTATCOM in distribution networks," *IEEE Transactions on Power Delivery*, vol. 33, no. 2, pp. 570-580, Apr. 2018.

[6] Q. Zhao, W. Liao, S. Wang *et al.*, "Robust voltage control considering uncertainties of renewable energies and loads via improved generative adversarial network," *Journal of Modern Power Systems and Clean Energy*, vol. 8, no. 6, pp. 1104-1114, Nov. 2020.

[7] R. Hossain, M. Gautam, M. MansourLakouraj *et al*., "Multi-agent deep reinforcement learning-based volt-var control in active distribution grids," in *Proceedings of 2023 IEEE PES General Meeting*, Orlando, USA, Jul. 2023, pp. 1-5.

[8] M. Koutenaei, T. Nguyen, T. Vu *et al*., "Efficient phasor-based dynamic volt/var and volt/WATT analysis of large distribution grid with high penetration of smart inverters," *IEEE Transactions on Smart Grid*, vol. 13, no. 5, pp. 3997-4008, Sept. 2022.

[9] C. Zhang, Y. Xu, Y. Wang *et al*., "Three-stage hierarchically-coordinated volt/var control based on PV inverters considering distribution network voltage stability," *IEEE Transactions on Sustainable Energy*, vol. 13, no. 2, pp. 868-881, Apr. 2022.

[10] Q. Ma and C. Deng, "Deterministic and robust volt-var control methods of power system based on convex deep learning," *Journal of Modern Power Systems and Clean Energy*, vol. 12, no. 3, pp. 719-729, May 2024.

[11] N. Shi, R. Cheng, L. Liu *et al*., "Data-driven affinely adjustable robust volt/var control," *IEEE Transactions on Smart Grid*, vol. 15, no. 1, pp. 247-259, Jan. 2024.

[12] K. Kumar, A. Mantha, and G. Ravikumar, "Bayesian optimization for deep reinforcement learning for robust volt/var control," in *Proceedings of 2024 IEEE PES General Meeting*, Seattle, USA, Jul. 2024, pp. 1-5.

[13] Y. Gao, W. Wang, and N. Yu, "Consensus multi-agent reinforcement learning for volt-var control in power distribution networks," *IEEE Transactions on Smart Grid*, vol. 12, no. 4, pp. 3594-3604, Jul. 2021.

[14] Y. Zhang, X. Wang, J. Wang *et al*., "Deep reinforcement learning based volt-var optimization in smart distribution systems," *IEEE Transactions on Smart Grid*, vol. 12, no. 1, pp. 361-371, Jan. 2021.

[15] Y. Tao, J. Qiu, S. Lai *et al*., "Distributed adaptive robust restoration scheme of cyber-physical active distribution system with voltage control," *IEEE Transactions on Power Systems*, vol. 39, no. 1, pp. 2170-2184, Jan. 2024.

[16] H. Liu, W. Shi, and H. Zhu, "Hybrid voltage control in distribution networks under limited communication rates," *IEEE Transactions on Smart Grid*, vol. 10, no. 3, pp. 2416-2427, May 2019.

[17] D. Molzahn, F. Dörfler, H. Sandberg *et al*., "A survey of distributed optimization and control algorithms for electric power systems," *IEEE Transactions on Smart Grid*, vol. 8, no. 6, pp. 2941-2962, Nov. 2017.

[18] F. Islam, A. Lallu, K. Mamun *et al*., "Power quality improvement of distribution network using BESS and capacitor bank," *Journal of Modern Power Systems and Clean Energy*, vol. 9, no. 3, pp. 625-632, Jun. 2021.

[19] R. Cheng, N. Shi, S. Maharjan *et al*., "Automatic self-adaptive local voltage control under limited reactive power," *IEEE Transactions on Smart Grid*, vol. 14, no. 4, pp. 2851-2862, Jul. 2023.

[20] N. Li, G. Qu, and M. Dahleh, "Real-time decentralized voltage control in distribution networks," in *Proceedings of 2014 52nd Annual Allerton Conference on Communication*, *Control*, *and Computing*, Monticello, USA, Sept. 2014, pp. 582-588.

[21] K. Antoniadou-Plytaria, I. Kouveliotis-Lysikatos, P. Georgilakis *et al*., "Distributed and decentralized voltage control of smart distribution networks: models, methods, and future research," *IEEE Transactions on Smart Grid*, vol. 8, no. 6, pp. 2999-3008, Nov. 2017.

[22] S. Bolognani, R. Carli, G. Cavraro *et al*., "Distributed reactive power feedback control for voltage regulation and loss minimization," *IEEE Transactions on Automatic Control*, vol. 60, no. 4, pp. 966-981, Apr. 2015.

[23] W. Zheng, W. Wu, B. Zhang *et al*., "A fully distributed reactive power optimization and control method for active distribution networks," *IEEE Transactions on Smart Grid*, vol. 7, no. 2, pp. 1021-1033, Mar. 2016.

[24] H. Liu, W. Shi, and H. Zhu, "Distributed voltage control in distribution networks: online and robust implementations," *IEEE Transactions on Smart Grid*, vol. 9, no. 6, pp. 6106-6117, Nov. 2018.

[25] E. Anese, S. Dhople, B. Johnson *et al*., "Decentralized optimal dispatch of photovoltaic inverters in residential distribution systems," *IEEE Transactions on Energy Conversion*, vol. 29, no. 4, pp. 957-967, Dec. 2014.

[26] C. Feng, Z. Li, M. Shahidehpour *et al*., "Decentralized short-term voltage control in active power distribution systems," *IEEE Transactions on Smart Grid*, vol. 9, no. 5, pp. 4566-4576, Sept. 2018.

[27] X. Zhou, S. Zou, P. Wang *et al*., "Voltage regulation in constrained distribution networks by coordinating electric vehicle charging based on hierarchical ADMM," *IET Generation*, *Transmission & Distribution*, vol. 14, no. 17, pp. 3444-3457, Sept. 2020.

[28] R. Cheng, N. Shi, and Z. Wang, "Fast ADMM-based hierarchical and decentralized volt/var control in distribution networks," in *Proceedings of 2022 IEEE PES General Meeting*, Denver, USA, Jul. 2022, pp. 1-5.

[29] Y. Guo, H. Gao, D. Wang *et al.*, "Online optimal feedback voltage control of wind farms: decentralized and asynchronous implementations," *IEEE Transactions on Sustainable Energy*, vol. 12, no. 2, pp. 1489-1492, Apr. 2021.

[30] J. Li, Z. Xu, J. Zhao *et al*., "Distributed online voltage control in active distribution networks considering PV curtailment," *IEEE Transactions on Industrial Informatics*, vol. 15, no. 10, pp. 5519-5530, Oct. 2019.

[31] W. Ma, J. Wang, V. Gupta *et al*., "Distributed energy management for networked microgrids using online ADMM with regret," *IEEE Transactions on Smart Grid*, vol. 9, no. 2, pp. 847-856, Mar. 2018.

[32] Y. Guo, H. Gao, and Z. Wang, "Distributed online voltage control for wind farms using generalized fast dual ascent," *IEEE Transactions on Power Systems*, vol. 35, no. 6, pp. 4505-4517, Nov. 2020.

[33] R. Cheng, Z. Wang, Y. Guo *et al*., "Online voltage control for unbalanced distribution networks using projected Newton method," *IEEE Transactions on Power Systems*, vol. 37, no. 6, pp. 4747-4760, Nov. 2022.

[34] T. Xu and W. Wu, "Accelerated ADMM-based fully distributed inverter-based volt/var control strategy for active distribution networks," *IEEE Transactions on Industrial Informatics*, vol. 16, no. 12, pp. 7532-7543, Dec. 2020.
[35] R. Cheng, Z. Wang, and Y. Guo, "An online feedback-based linearized power flow model for unbalanced distribution networks," *IEEE Transactions on Power Systems*, vol. 37, no. 5, pp. 3552-3565, Sept. 2022.
[36] P. Giselsson and S. Boyd, "Metric selection in fast dual forward–backward splitting," *Automatica*, vol. 62, pp. 1-10, Dec. 2015.
[37] P. Giselsson and S. Boyd, "Diagonal scaling in Douglas-Rachford splitting and ADMM," in *Proceedings of 53rd IEEE Conference on Decision and Control*, Los Angeles, USA, Dec. 2014, pp. 5033-5039.

Heshi Wang received the B.S. degree in smart grid information engineering from North China Electric Power University, Beijing, China, in 2022. He is currently working toward the Ph.D degree with the School of Electric and Electronic Engineering, North China Electric Power University. His main research interests include power distribution system, volt/var control, and application of flexibility resource in grid resilience enhancement.

Wenxia Liu received the B.S. degree in radio technology from Nanjing University of Science and Technology, Nanjing, China, in 1990, the M.S. degree in electrical engineering and automation from Northeast Electric Power University, Jilin, China, in 1995, and the Ph.D. degree in electrical engineering and automation from North China Electric Power University, Beijing, China, in 2009. She is currently a Professor in a School of Electric and Electronic Engineering, North China Electric Power University. Her research interests include risk assessment in power system and security in cyber-physical power system.

Rui Cheng received the Ph.D. degree in electrical engineering from Iowa State University, Ames, USA, in 2023. He is currently an Assistant Professor with North China Electric Power University, Beijing, China. His research interests include optimization and machine learning in distribution system, and power system vulnerability and reliability.

Fuxin Wang received the B.S. degree in electrical engineering and automation from Changsha University of Science and Technology, Changsha, China, in 2023. She is currently working toward the M.S. degree with the School of Electric and Electronic Engineering, North China Electric Power University, Beijing, China. Her main research interests include risk assessment of power system and resilience analysis of power system under extreme weather.

Tianlong Wang received the B.S. degree in electrical engineering and automation from North China Electric Power University, Beijing, China, in 2023. He is currently working toward the Ph.D degree with the School of Electric and Electronic Engineering, North China Electric Power University. His main research interests include power system operation and control, power system reliability analysis, and risk assessment.